



Realizing a high-efficiency 426nm laser with PPKTP by reducing mode-mismatch caused by the thermal effect

QINGWEI WANG,¹ LONG TIAN,^{1,2} WENXIU YAO,¹ YAJUN WANG,^{1,2} 
AND YAOHUI ZHENG^{1,2,*} 

¹State Key Laboratory of Quantum Optics and Quantum Optics Devices, Institute of Opto-Electronics, Shanxi University, Taiyuan 030006, China

²Collaborative Innovation Center of Extreme Optics, Shanxi University, Taiyuan 030006, China

*yhzheng@sxu.edu.cn

Abstract: We report on a high conversion efficiency tunable laser at 426 nm by adopting an external frequency-doubling cavity pumped by a diode laser. For the frequency-doubling process at 426 nm, the major challenge of increasing the conversion efficiency is mode-match degradation originating from the severely thermal effect. Here, we find that the center of the equivalently thermal lens is not at the center of the nonlinear crystal. We minimize the variation of beam parameters of the Gaussian beam in the external cavity by optimizing the center of the thermal lens to beam waist. As a result, the mode-match degradation is reduced as the incident power is increased. Finally, a 405 mW blue light is obtained with the conversion efficiency of 81%.

© 2019 Optical Society of America under the terms of the [OSA Open Access Publishing Agreement](#)

1. Introduction

Second harmonic generation (SHG) is employed for obtaining continuous wave laser at various wavelengths for lots of applications, such as biomedicine, spectroscopy and quantum optics. In the field of quantum optics, SHG is widely used to prepare pump beams of optical parametric oscillator, generating nonclassical states including squeezed states [1–7] and entangled states [8,9] which are indispensable resources for building quantum interface and quantum internet [10]. Such quantum network consists of quantum channels for transforming quantum states and quantum nodes for generating, storing and processing the quantum states [11,12]. A controllable quantum system with alkali atoms or solid state systems provides a versatile interface to store and manipulate the quantum information [13–16]. Collective excitations of cesium (Cs) ensemble can realize high-speed quantum memory [17], which is a contemporary challenge for quantum technologies. Therefore, the high-efficiency generation of a continuous-wave single-frequency blue laser and further realization of high performance nonclassical states resonant on Cs D_2 line at 852 nm is essential to light-atom interaction [18,19], atomic entanglement generation [18] and ultra-precise measurement [20]. However, the significant alkali atomic transitions (rubidium and Cs) are usually near-infrared, thus the harmonic wave (HW) of these corresponding transition lines are in ultra-violet and blue regime [21–23]. Furthermore, the SHG laser should satisfy the continuously tunable condition to resonant with the atomic transition line.

In the aspect of frequency doubling at around Cs D_2 line 852 nm, Polzik obtained 650 mW of blue light at 430 nm with a fundamental wave (FW) power of 1.35 W by using a KNbO_3 crystal in an optical ring cavity with the conversion efficiency of 48% [24]. In 2006, Suzukl et al reported on 400 mW blue light at 430 nm with KNbO_3 with an incident power of 900 mW [25]. For SHG at around 852 nm, periodically poled potassium titanyl phosphate (PPKTP) is another attractively nonlinear crystal because of its relatively high effective nonlinear coefficients, high damage threshold and no walk-off effect. Villa et al generated 330 mW blue light at 426 nm laser by using a ring cavity with a PPKTP crystal, corresponding to the conversion efficiency of 55%

[23]. A monolithic PPKTP cavity was used in frequency doubling at 852 nm, achieving 158 mW blue light output (45%) [26]. Recently, 210 mW blue light at 426 nm was obtained by using a 20 mm-long PPKTP crystal in a ring cavity, corresponding to the conversion efficiency of 67% [27]. It is worthy of noting that all these works mentioned above were finished by using a Ti:sapphire laser.

Diode lasers (DL) have advantages of compact structure, low cost and easy operation, large ranges of wavelengths including many significant atomic transitions. Based on these reasons, diode-laser-based SHG would greatly extend the range of SHG experiments. We can easily tune the wavelength of the DL by adjusting the temperature and the injection current of the DL and then address atomic transitions. However, the relatively poor beam quality of the DL limits the conversion efficiency [28,29], with the maximum net value of 75% under the consideration of mode-matching efficiency [28].

The thermal effect originating from the crystal absorption for circulating light is a main limit factor of further increasing the conversion efficiency and stability at high output power [30,31]. The effect is more serious especially at short wavelength due to blue light induced infrared absorption (BLIIRA) and strong absorption for blue light, which induces the phase mismatching of nonlinear interaction, mode mismatching of the FW. In order to increase the conversion efficiency, we must reduce the thermal effect and mode-mismatching as far as possible during the period of increasing the incident power. In general, the thermal effect can be reduced by relaxing the focusing parameter of frequency-doubling cavity and the geometry center of the crystal is overlapped with the beam waist for increasing the conversion efficiency [28]. Here, we expect to reduce the variation of mode-matching efficiency under the thermal effect invariance. Based on the transformation of Gaussian beam, the change of the beam parameters can be omitted when the center of the equivalent thermal lens is located at the waist of the beam, especially for Gaussian beam with small waist. While the change of the beam parameters becomes obvious with the position deviation, which induces the mode mismatching. The center of thermal lens is not the geometry center of the crystal, but has a deviation, dependent of the thermal distribution. So there requires to quantify the center of the equivalent thermal lens, optimizing the crystal position to minimize the variation of the beam parameters. However, there has no regard for the influence of the crystal position on the mode-mismatch.

In this paper, we report on a high conversion efficiency blue laser at 426 nm with a conversion efficiency up to 81% with a DL as incident beam. To our knowledge, this is the highest efficiency for SHG around Cs D_2 line with an external ring cavity so far. By theoretically analyzing the thermal lensing effect and the induced mode mismatching, we point out that the center of the equivalent thermal lens is not at the center of the crystal, but with a deviation. In combination with the transformation of Gaussian beam, we adjust that the center of the thermal lens coincides with the waist, to reduce the mode-mismatching and increase the conversion efficiency. The output power of blue laser can reach up to 405 mW when 500 mW FW is injected. The corresponding power fluctuation is 3.5% (1.3%) for 1 hour at an input power of 500 mW (370 mW). Furthermore, we develop a self-lock technique to realize the generated 426 nm laser can be continuously tuned about 8 GHz by changing the frequency of FW, which covers the $(6^2S_{1/2}, F = 4) \rightarrow (6^2P_{3/2}, F' = 3) - (6^2S_{1/2}, F = 4) \rightarrow (6^2P_{3/2}, F' = 5)$ transitions of Cs D_2 line. We believe that the high-efficiency tunable blue laser at 426 nm will provide an ideal light source for generating stably non-classical states of light resonant with the Cs atom D_2 absorption line.

2. Theoretical analysis

The thermal effect in the nonlinear crystal can seriously affect the conversion efficiency of the SHG, which should be thoroughly considered to achieve a high conversion efficiency.

Without the thermal lensing. The overall conversion efficiency of the cavity is $\eta = P_{out}/P_{in}$ and the output power of the SHG is $P_{out} = E_{NL} \cdot P_c^2$. P_{in} is the incident power, P_c represents the enhancement of resonant FW power for a ring cavity, can be written as [32]:

$$P_c = \frac{P_{in} \cdot T_1}{\left[1 - \sqrt{(1 - T_1)(1 - L)(1 - \Gamma \cdot P_c)}\right]^2}. \quad (1)$$

Where, T_1 is the transmission of the input coupler of the ring cavity and L is the round-trip loss of the FW in the cavity without T_1 . Γ contains all the nonlinear losses and can be written as the sum as $\Gamma = E_{NL} + \Gamma_{abs}$. The first part E_{NL} is the single pass conversion efficiency of the PPKTP crystal and the other part Γ_{abs} represents the efficiency of the second harmonic generation absorption process inside the crystal. E_{NL} is given by the well-known Boyd and Kleinman expression [33]:

$$E_{NL} = \frac{4\omega^2 d_{eff}^2 L_c}{\varepsilon_0 c^3 \lambda_1 n_1 n_2} h(\alpha, \xi, \sigma) \exp[-(\alpha_1 + \alpha_2/2)L_c], \quad (2)$$

$$h(\alpha, \xi, \sigma) = \frac{1}{2\xi} \int_{-\xi/2}^{+\xi/2} \int_{-\xi/2}^{+\xi/2} dt dt' \frac{\exp[-\alpha(t+t'+\xi) - i\sigma(t-t')]}{(1+it)(1-it')}. \quad (3)$$

Where, ω is the angle frequency of the FW, d_{eff} is the effective nonlinear coefficient, c is the light velocity in vacuum, ε_0 is the vacuum dielectric constant, L_c is the length of the crystal, n_1 and n_2 are the refraction index of FW and HW, respectively. α_1 and α_2 are the linear absorption coefficients of FW and HW, respectively. α equals to $(\alpha_1 - \alpha_2/2)z_R$ and h is the Boyd-Kleinman focusing factor which depends on the focusing parameter $\xi = L_c/z_R$, where z_R is the Gaussian beam Rayleigh length. σ represents the wave-vector mismatch. The parameters taken here are: $n_1=1.84$, $n_2=1.94$, $\alpha_1 = 1\%cm^{-1}$, $\alpha_2 = 10\%cm^{-1}$, $\varepsilon_0 = 8.85 \times 10^{-12}F/m$, and $d_{eff} = (2/\pi)d_{33} \approx 9.5pm/V$. Based on these parameters, we theoretically calculate the conversion efficiency versus input power without considering the mode-mismatching induced by thermal lens effects, shown in Fig. 5.

With the thermal lensing, we assume that thermal lensing is the only side effect of thermal effects. The thermal focus length caused by the temperature gradient can be expressed as [34]:

$$f = \frac{\pi K_c \omega_0^2}{P_{out} (dn/dT)} \frac{1}{1 - e^{-(\alpha_1 + \alpha_2/2)L_c}}. \quad (4)$$

Where, K_c is the thermal conductivity, ω_0 is the waist radius of the cavity, dn/dT is the thermo-optic coefficient with the parameters $K_c = 3.3W/(m^\circ C)$, $dn/dT = 15.3 \times 10^{-6}K^{-1}$. When the input power changes from 0 to 1 W, the thermal focus length located in the cavity changes from ∞ to 28 mm. It is obvious that the thermal effect is extremely serious at short wavelength, which should be thoroughly quantified and considered.

As the light power illuminated in the crystal changes, the cavity mode size is dependent of the thermal lensing change. The external cavity is optimally mode matched with the FW without the thermal lensing. The cavity mode variation will inevitably degrade the mode matching efficiency. It is necessary to minimize the variation of mode matching efficiency during the variation of the incident power to increase the conversion efficiency. Based on the transformation of Gaussian beam, the change of the beam parameters can be omitted with the focal length variation of a lens, especially for Gaussian beam with small waist, when the waist of Gaussian beam coincides in position with the center of the lens. According to the above analysis, it is necessary to locate the center of the equivalent thermal lens.

The thermal lens originates from the temperature gradient from the axis to the edge that is related to the heat accumulation. The power density along the crystal axis represents the thermal distribution, and the position of the maximum power density can be considered to the center of

the thermal lens. We calculate the power density along the axis in the crystal, and the results show that the position of maximum power density is not at the center of the crystal, but with a deviation. The calculation results is shown in Fig. 1, Figs. 1(a), 1(b) and 1(c) represent the power density distribution along the crystal axis with a beam waist of $32\ \mu\text{m}$, $36\ \mu\text{m}$, $40\ \mu\text{m}$, respectively. The position of the maximum power density deviates further and further away from the central point of the crystal with the increasing of beam waist. The deviation induces a large cavity mode size change that degrades the mode match between the FW and frequency doubling cavity. Figure 1(d) shows the power density distribution along the axis after optimizing the crystal position with a beam waist of $36\ \mu\text{m}$. The optimization does not only reduce the maximum power density, but also coincide the position of the thermal lens with the beam waist.

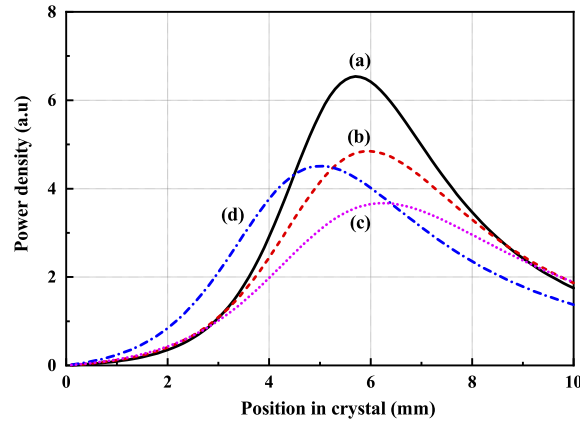


Fig. 1. Power density distribution along the crystal axis with different beam waists: (a) $32\ \mu\text{m}$, (b) $36\ \mu\text{m}$, (c) $40\ \mu\text{m}$. (d) is the new power density distribution along the axis after optimizing the crystal position with a beam waist of $36\ \mu\text{m}$.

Substitute Eq. (4) into the ABCD matrix of the cavity, we can get the size and position of the waist in the cavity. The mode-matching efficiency to the cavity TEM_{00} mode can be written as [35,36]:

$$\kappa_{00} = \frac{16 \prod_{\alpha=x,y} \left\{ \int_0^l \frac{1}{W_{\alpha}^2(z) + W_{\alpha,e}^2(z)} dz \right\}^2}{\prod_{\alpha} \left\{ \int_0^l \frac{1}{W_{\alpha}^2(z)} dz \right\} \left\{ \int_0^l \frac{1}{W_{\alpha,e}^2(z)} dz \right\}}, \quad (5)$$

in which $W_{\alpha}(z)$ can be expressed to

$$W_{\alpha}^2(z) = W_{\alpha 0}^2 \left\{ 1 + \left(\frac{z - z_{\alpha}}{z_{\alpha 0}} \right)^2 \right\}, \quad (6)$$

$$z_{\alpha 0} = \pi W_{\alpha 0}^2 / \lambda. \quad (7)$$

Where, $W_{\alpha}(z)$ and $W_{\alpha 0}$ is the beam radius at $1/e$ of the amplitude and the beam radius of the incident beam at the waist position $z = z_{\alpha}$, respectively; $W_{\alpha,e}(z)$ and $W_{\alpha,e 0}$ are that of the cavity eigenmodes. Considering the effect of mode-mismatching caused by thermal lens, the relation between the conversion efficiency and the input power is shown in Fig. 5. Compared with the conversion efficiency without thinking about the effect of thermal lens, it is obvious that the conversion efficiency gets to be lower with the increase of the incident power.

The nonlinear crystal is usually placed in the midpoint of two concave mirrors (the position of cavity mode) for ring cavity. However, the power of the generated blue light will be gradually increased with the spread of FW in the crystal, the maximum value of power density is now at

the center of the crystal. According to the transformation of Gaussian beam, the change of the beam parameter can be omitted with the focal length of the thermal lens, especially for Gaussian beam with small waist, when the waist of Gaussian beam coincides in position with the center of the thermal lens. In order to minimize the variation of beam parameter, we should optimize the crystal position and make the center of thermal lens coincide with the waist position. The variation of the cavity mode is calculated before and after the optimization, shown in Fig. 2. The results reveal that the mode waist size is more sensitive to the incident power before the optimization than that of after the optimization. Further, we analyze and obtain the relationship between mode-matching efficiency of the incident power before and after the optimization, shown in Fig. 3. For the input power range from 0 to 1 W, the mode-matching efficiency decreases from 98% to 96.7% after the optimization, to 88.9% before the optimization. So the optimization process can effectively reduce the variation of the mode-matching efficiency, which is benefit of increasing the conversion efficiency.

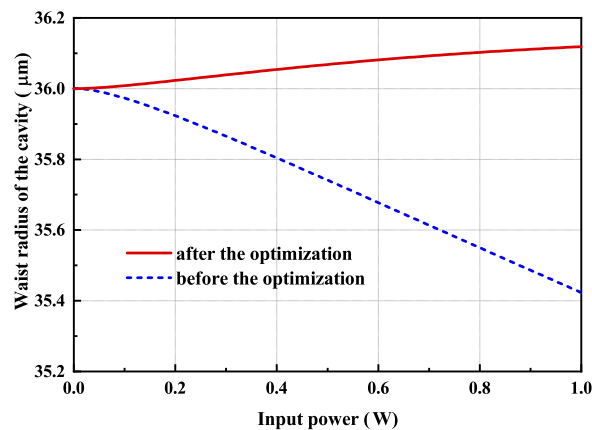


Fig. 2. Variation of the waist radius with the incident power. Solid line: after the optimization; Dashed line: before the optimization.

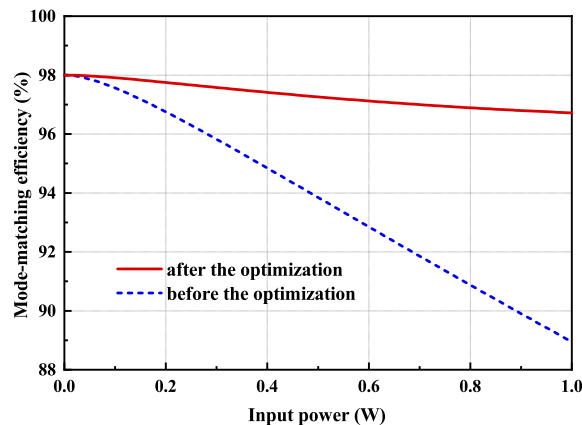


Fig. 3. Mode-matching efficiency as the input FW power. Solid line: after the optimization; Dashed line: before the optimization.

3. Experimental setup

Following the above analysis, we carry out the experiment. The schematic of our experimental setup is shown in Fig. 4. We adopt a continuous-wave diode laser with the center wavelength of 852 nm, corresponding to the D_2 transition of Cs atoms, as the laser source (Toptica Photonics AG DL pro). The laser emitted from DL is injected into a tapered amplifier (TA) to generate a high-power laser source (Toptica Photonics AG BossTA pro). A polarization-maintaining single-mode fiber is used to improve the spatial mode of the beam, and an optical isolator (OI) is used to avoid back-reflected light. A wedged electro-optic modulator (EOM) is used to generate the error signals of the Pound-Drever-Hall (PDH) sideband locking technique [37]. After the EOM, the beam is split into two parts by a half-wave-plate (HWP) and a polarization beam splitter (PBS). The reflected light from the PBS is injected into a saturated absorption spectroscopy to get the absorption signal to control the frequency of the DL. A HWP and a PBS is used to regulate the power of transmitted light of the first PBS. Lens L1 and L2 are placed in the light path to match the mode into the cavity and the original mode-matching efficiency was measured to be about 98% in our experiment.

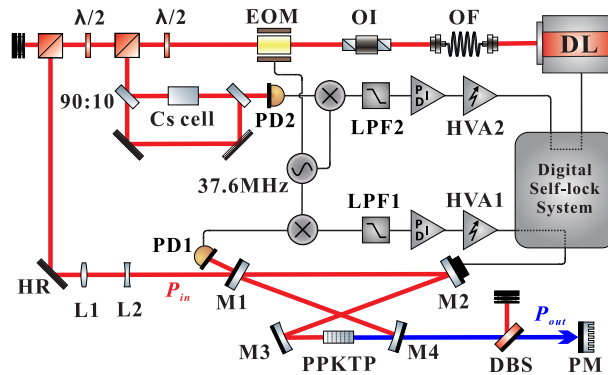


Fig. 4. Experimental setup. DL, diode laser; OF, optical fiber; OI, optical isolator; EOM, electro-optic modulator; PD1-2, photodetector; LPF1-2, low-pass filter; PID, proportional-integral-derivative; HVA1-2, high-voltage amplifier; HR, high-reflection mirror; DBS, dichroic beam splitter; PM, power meter.

We use a symmetrical bow-tie ring cavity as the SHG cavity, the cavity consists of four mirrors, in which M1 and M2 are plane mirrors, M3 and M4 are concave mirrors. M3 and M4 have a radius of curvature of 100 mm with reflectivity of 99.995% at the FW. The transmission of the input coupler mirror M1 is 12.5%. A PZT is bonded to the highly reflective mirror M2, serving as the control component. The total length of the cavity is 608 mm and the distance between the two concave mirrors is 108 mm. A PPKTP crystal (Raicol Crystals Ltd.) with the dimensions of $1\text{mm} \times 2\text{mm} \times 10\text{mm}$ is placed between two concave mirrors, the position is carefully adjusted by a displacement stage (Newport MS-125-X) to make the center of the thermal lens coincide with the waist between two concave mirrors, aiming to reduce the mode-mismatch. The displacement stage has a resolution of 0.01mm, which is enough to meet the requirement for the optimization. The poling period of the crystal is $4.5\ \mu\text{m}$ and the crystal is temperature stabilized by a temperature controller with a measurement precision $0.002\ ^\circ\text{C}$. Two low-noise, transformer-coupled resonant photodetectors are used to get error signal with high signal-noise ratio [38]. A high frequency signal (37.6 MHz) generated by a function generator is divided into three parts, one is used to drive the EOM and the other two are mixed with the detected signal by using two mixers. The output of two mixers are PDH error signals as controlling the cavity length of external frequency-doubling cavity, stabilizing the frequency of the DL. After low-pass filter, proportional-integral-derivative

(PID) controller and high-voltage amplifier (HVA), two error signals are feedback to control unit. The output laser of the cavity consists of generated blue laser and a tiny part of infrared laser, a dichroic beam splitter (DBS) is used to separate the two lights. A power meter (Thorlabs S130C) is used to measure the power of the output beam at 426 nm. A digital self-lock system is used to ensure that the frequency-doubling cavity operates continuously during frequency tuning. The output blue laser can be tuned with 8 GHz frequency range by scanning the incident infrared laser over $(6^2S_{1/2}, F = 4) \rightarrow (6^2P_{3/2}, F' = 3) \rightarrow (6^2S_{1/2}, F = 4) \rightarrow (6^2P_{3/2}, F' = 5)$ transitions of Cs D_2 line.

The laser has a maximum output power of 460 mW. The measured performance of output power of the HW is shown in Fig. 5. The discrete points are the measured experimental data, real lines are calculation results. Usually, the geometry center of the crystal is overlapped with the beam waist, which represents the status before optimization. According to our calculation, the center of the equivalent thermal lens has a 1.01 mm deviation from that of the crystal. We move the crystal position to make the center of the thermal lens overlap with the beam waist, corresponding to the status after optimization. During the optimization process, the crystal displacement is approximately 1.03 mm, which is in good agreement with the calculation one. It is obvious that the conversion efficiency after the optimization is higher than that of before the optimization. In low power region, the experimental results have very slight deviation from the calculation one, which confirms that the theoretical model is correct. As the incident power is increased, the deviation increases gradually, which can be attributed to the gradually enhanced BLIIRA with the laser power at 426 nm [39]. Unfortunately, there is lack of an additional blue light to quantify the relationship between BLIIRA and blue light intensity. So we don't consider the BLIIRA in the theoretical model.

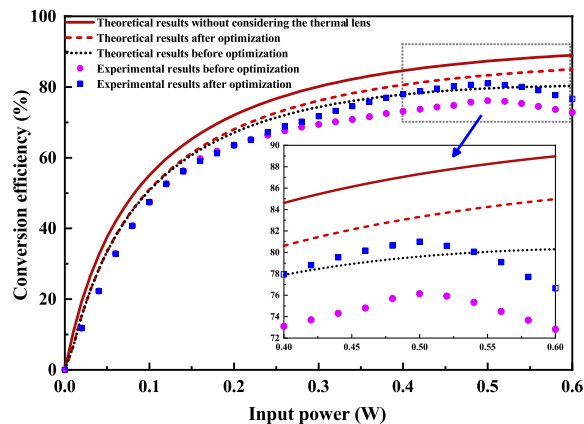


Fig. 5. Theoretical and experimental conversion efficiencies. Brown solid line is the theoretical result without considering thermal lens. Red dotted line and black dashed line are theoretical results after and before the optimization, respectively. Blue squares and carmine circles are experimental results after and before the optimization, respectively.

Subsequently, we measure the power of the FW in front of the frequency-doubling cavity P_{in} , the power of the HW after the DBS P_{out} . The conversion efficiency is the ratio of P_{in} to P_{out} . A maximum conversion efficiency of 81% is obtained at the input power of 500 mW after the optimization, the maximum conversion efficiency is 76% before the optimization. The 426 nm output laser has a good power stability of the output laser is measured at 280 mW, 370 mW and 500 mW for over 1h in continuous wave mode and the root mean square (RMS) fluctuation is 0.8%, 1.3% and 3.5% respectively. The results are shown in Fig. 6. The thermal effect originating from BLIIRA is main reason of the variation of the output power with time. Ref. [39] has studied

the evolution of BLIIRA with time, which further confirms our explanation. The additional intracavity loss and nonlinear phase mismatching coming from BLIIRA is the direct reason of the power degradation. The output power can recover after the PPKTP relax for some time, which is in good agreement with the Ref. [39]. This is another evidence that the influence of BLIIRA on the power fluctuation occurs. As shown in Fig. 7, the output blue laser is still stable while detuning the FW over 4GHz, the inferred range for the HW is 8 GHz.

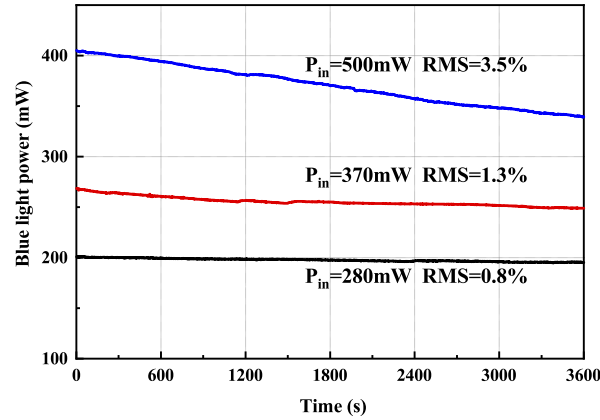


Fig. 6. Power stability of the HW output with different input FW power.

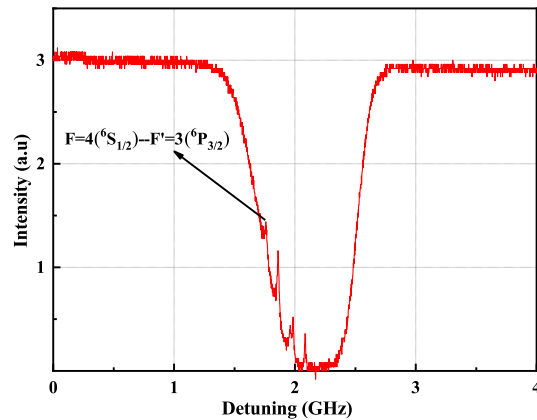


Fig. 7. Saturation absorption spectroscopy of $(6^2S_{1/2}, F = 4) \rightarrow (6^2P_{3/2}, F' = 3)$ — $(6^2S_{1/2}, F = 4) \rightarrow (6^2P_{3/2}, F' = 5)$ transitions of Cs D_2 line when the infrared diode laser is scanned.

4. Conclusion

In conclusion, we report on a tunable blue laser at 426 nm by adopting an external frequency-doubling cavity pumped by a diode laser, with a conversion efficiency up to 81%, with a maximum output power of 460 mW. By theoretically analyzing the thermal lensing effect and the induced mode mismatching, we draw a conclusion that the center of the equivalent thermal lens is not at the center of the crystal, but with a deviation. By comparing the variation of waist size, mode-matching efficiency, conversion efficiency before and after the optimization, we confirm that the conversion efficiency can be effectively increased by optimizing the crystal position. In

experiment, we adjust that the center of the thermal lens coincides with the waist, to reduce the mode-mismatching and increase the conversion efficiency. Before this, no one systematically analyzes these questions. We believe that the output power is strong enough to generate the continuous variable squeezed states at 852 nm resonant with the D_2 line of Cs atoms (Threshold power at Ref. [25]: 180 mW). The conversion efficiency we have obtained is so far, to the best of our knowledge, the highest-reported one at this wavelength. The tuning range of the SHG can be expanded to 8 GHz with a digital self-lock system.

Funding

National Natural Science Foundation of China (61575114, 11654002, 11804207, 11874250); Program for Sanjin Scholar of Shanxi Province; Program for Outstanding Innovative Teams of Higher Learning Institutions of Shanxi; Fund for Shanxi "1331 Project" Key Subjects Construction; (2016YFA0301401); Natural Science Foundation of Shanxi Province (201801D221006).

References

1. M. S. Stefszky, C. M. M. Lowry, S. S. Y. Chua, D. A. Shaddock, B. C. Buchler, H. Vahlbruch, A. Khalaidovski, R. Schnabel, P. K. Lam, and D. E. McClelland, "Balanced homodyne detection of optical quantum states at audio-band frequencies and below," *Class. Quantum Gravity* **29**(14), 145015 (2012).
2. S. Burks, J. Ortalo, A. Chiummo, X. Jia, F. Villa, A. Bramati, J. Laurat, and E. Giacobino, "Vacuum squeezed light for atomic memories at the D_2 cesium line," *Opt. Express* **17**(5), 3777 (2009).
3. H. Vahlbruch, M. Mehmet, K. Danzmann, and R. Schnabel, "Detection of 15 dB squeezed states of light and their application for the absolute calibration of photoelectric quantum efficiency," *Phys. Rev. Lett.* **117**(11), 110801 (2016).
4. W. H. Yang, S. P. Shi, Y. J. Wang, W. G. Ma, Y. H. Zheng, and K. C. Peng, "Detection of stably bright squeezed light with the quantum noise reduction of 12.6 dB by mutually compensating the phase fluctuations," *Opt. Lett.* **42**(21), 4553 (2017).
5. S. P. Shi, Y. J. Wang, W. H. Yang, Y. H. Zheng, and K. C. Peng, "Detection and perfect fitting of 13.2 dB squeezed vacuum states by considering green-light-induced infrared absorption," *Opt. Lett.* **43**(21), 5411 (2018).
6. W. H. Yang, X. L. Jin, X. D. Yu, Y. H. Zheng, and K. C. Peng, "Dependence of measured audio-band squeezing level on local oscillator intensity noise," *Opt. Express* **25**(20), 24262 (2017).
7. X. C. Sun, Y. J. Wang, L. Tian, S. P. Shi, Y. H. Zheng, and K. C. Peng, "Dependence of the squeezing and anti-squeezing factors of bright squeezed light on the seed beam power and pump beam noise," *Opt. Lett.* **44**(7), 1789 (2019).
8. T. Eberle, V. Handchen, and R. Schnabel, "Stable control of 10 dB two-mode squeezed vacuum states of light," *Opt. Express* **21**(9), 11546 (2013).
9. S. Ast, M. Ast, M. Mehmet, and R. Schnabel, "Gaussian entanglement distribution with gigahertz bandwidth," *Opt. Lett.* **41**(21), 5094 (2016).
10. H. J. Kimble, "The quantum internet," *Nature* **453**(7198), 1023–1030 (2008).
11. Y. H. Liu, J. L. Yan, L. X. Ma, Z. H. Yan, and X. J. Jia, "Continuous-variable entanglement distillation between remote quantum nodes," *Phys. Rev. A* **98**(5), 052308 (2018).
12. Z. H. Yan and X. J. Jia, "Quantum manipulation and enhancement of deterministic entanglement between atomic ensemble and light via coherent feedback control," *Quantum Sci. Technol.* **2**(2), 024003 (2017).
13. Z. H. Yan, L. Wu, X. J. Jia, Y. H. Liu, R. J. Deng, S. J. Li, H. Wang, C. D. Xie, and K. C. Peng, "Establishing and storing of deterministic quantum entanglement among three distant atomic ensembles," *Nat. Commun.* **8**(1), 718 (2017).
14. K. Jensen, W. Wasilewski, H. Krauter, T. Fernholz, B. M. Nielsen, M. Owari, M. B. Plenio, A. Serafini, M. M. Wolf, and E. S. Polzik, "Quantum memory for entangled continuous-variable states," *Nat. Phys.* **7**(1), 13–16 (2011).
15. K. Hammerer, A. S. Sørensen, and E. S. Polzik, "Quantum interface between light and atomic ensembles," *Rev. Mod. Phys.* **82**(2), 1041–1093 (2010).
16. H. Y. Hao, L. Tian, H. X. Yuan, S. J. Li, and H. Wang, "The Experimental Investigation of 795 nm Correlation Photons caused by Spontaneous Parametric Down-Conversion," *Acta Sinica Quantum Opt.* **20**, 177–182 (2014).
17. K. F. Reim, J. Nunn, V. O. Lorenz, B. J. Sussman, K. C. Lee, N. K. Langford, D. Jaksch, and I. A. Walmsley, "Towards high-speed optical quantum memories," *Nat. Photonics* **4**(4), 218–221 (2010).
18. J. Hald, J. L. S. Sørensen, C. Schori, and E. S. Polzik, "Spin squeezed atoms: a macroscopic entangled ensemble created by light," *Phys. Rev. Lett.* **83**(7), 1319–1322 (1999).
19. Q. A. Turchette, N. Ph. Georgiades, C. J. Hood, and H. J. Kimble, "Squeezed excitation in cavity QED: Experiment and theory," *Phys. Rev. A* **58**(5), 4056–4077 (1998).
20. H. Krauter, D. Salart, C. A. Muschik, J. M. Petersen, H. Shen, T. Fernholz, and E. S. Polzik, "Deterministic quantum teleportation between distant atomic objects," *Nat. Phys.* **9**(7), 400–404 (2013).

21. Y. Zhang, J. H. Liu, J. Z. Wu, R. Ma, D. Wang, and J. X. Zhang, "Single-frequency tunable 447.3 nm laser by frequency doubling of tapered amplified diode laser at cesium D_1 line," *Opt. Express* **24**(17), 19769–19775 (2016).
22. X. Wen, Y. S. Han, J. D. Bai, J. He, Y. H. Wang, B. D. Yang, and J. Wang, "Cavity-enhanced frequency doubling from 795nm to 397.5nm ultra-violet coherent radiation with PPKTP crystals in the low pump power regime," *Opt. Express* **22**(26), 32293 (2014).
23. F. Villa, A. Chiummo, E. Giacobino, and A. Bramati, "High-efficiency blue-light generation with a ring cavity with periodically poled KTP," *J. Opt. Soc. Am. B* **24**(3), 576 (2007).
24. E. S. Polzik and H. J. Kimble, "Frequency doubling with KNbO_3 in an external cavity," *Opt. Lett.* **16**(18), 1400 (1991).
25. S. Suzuki, H. Yonezawa, F. Kannari, M. Sasaki, and A. Furusawa, "7dB quadrature squeezing at 860 nm with periodically poled KTiOPO_4 ," *Appl. Phys. Lett.* **89**(6), 061116 (2006).
26. X. Deng, J. Zhang, Y. C. Zhang, G. Li, and T. C. Zhang, "Generation of blue light at 426 nm by frequency doubling with a monolithic periodically poled KTiOPO_4 ," *Opt. Express* **21**(22), 25907 (2013).
27. J. F. Tian, C. Yang, J. Xue, Y. C. Zhang, G. Li, and T. C. Zhang, "High-efficiency blue light generation at 426 nm in low pump regime," *J. Opt.* **18**(5), 055506 (2016).
28. R. Le Targat, J.-J. Zondy, and P. Lemonde, "75%-Efficiency blue generation from an intracavity PPKTP frequency doubler," *Opt. Commun.* **247**(4-6), 471–481 (2005).
29. J. H. Lundeman, O. B. Jensen, P. E. Andersen, S. Andersson-Engels, B. Sumpf, G. Erbert, and P. M. Petersen, "High power 404 nm source based on second harmonic generation in PPKTP of a tapered external feedback diode laser," *Opt. Express* **16**(4), 2486 (2008).
30. F. Torabi-Goudarzi and E. Riis, "Efficient cw high-power frequency doubling in periodically poled KTP," *Opt. Commun.* **227**(4-6), 389–403 (2003).
31. L. L. Tan, J. C. Mauro, S. H. Xu, Z. M. Yang, and M. Y. Peng, "Unusual thermal response of tellurium near-infrared luminescence in phosphate laser glass," *Opt. Lett.* **43**(19), 4823 (2018).
32. A. Ashkin, G. D. Boyd, and J. M. Dziedzic, "Resonant Optical Second Harmonic Generation and Mixing," *IEEE J. Quantum Electron.* **2**(6), 109–124 (1966).
33. G. D. Boyd and D. A. Kleinman, "Parametric interaction of focused Gaussian light beams," *J. Appl. Phys.* **39**(8), 3597–3639 (1968).
34. M. E. Innocenzi, H. T. Yura, C. L. Fincher, and R. A. Fields, "Thermal modeling of continuous-wave end-pumped solid-state lasers," *Appl. Phys. Lett.* **56**(19), 1831–1833 (1990).
35. N. Uehara, E. K. Gustafson, M. M. Fejer, and R. L. Byer, "Modeling of efficient mode matching and thermal-lensing effect on a laser-beam coupling into a mode-cleaner cavity," *Proc. SPIE* **2989**, 57–68 (1997).
36. W. H. Yang, Y. J. Wang, Y. H. Zheng, and H. D. Lu, "Comparative study of the frequency-doubling performance on ring and linear cavity at short wavelength region," *Opt. Express* **23**(15), 19624 (2015).
37. Z. X. Li, W. G. Ma, W. H. Yang, Y. J. Wang, and Y. H. Zheng, "Reduction of zero baseline drift of the Pound-Drever-Hall error signal with a wedged electro-optical crystal for squeezed state generation," *Opt. Lett.* **41**(14), 3331 (2016).
38. C. Y. Chen, S. P. Shi, and Y. H. Zheng, "Low-noise, transformer-coupled resonant photodetector for squeezed state generation," *Rev. Sci. Instrum.* **88**(10), 103101 (2017).
39. S. Wang, V. Pasiskevicius, and F. Laurell, "Dynamics of green light-induced infrared absorption in KTiOPO_4 and periodically poled KTiOPO_4 ," *J. Appl. Phys.* **96**(4), 2023–2028 (2004).